

**A Thermobaric Instability of Lagrangian Vertical
Coordinate Ocean Models**

ROBERT HALLBERG

NOAA Geophysical Fluid Dynamics Laboratory, Princeton, New Jersey

Submitted to Ocean Modelling, October 29, 2003; in revised form December 19, 2003

Corresponding author address: Robert Hallberg, NOAA GFDL, Princeton University,
Forrestal Campus, U.S. Rt. 1, P.O. Box 308, Princeton, NJ 08542

E-mail: Robert.Hallberg@noaa.gov

ABSTRACT

Lagrangian- (and isopycnic-) vertical coordinate ocean models are subject to an exponentially growing numerical instability in weakly stratified regions when thermobaricity is not accurately compensated. Inaccurate compensation for compressibility in the pressure gradient terms leads to pressure gradient truncation errors (due to the vertical discretization) that can drive the Lagrangian coordinate surfaces to reinforce these errors. It is possible to avoid this instability while using the full nonlinear equation of state for seawater by using an optimal alternate discretization of the pressure gradient terms and extracting a slowly spatially varying reference compressibility that approximates the compressibility of the ocean's mean state.

1. Introduction

The full nonlinear equation of state is trivial to incorporate into ocean models cast in Eulerian vertical coordinates. Potential temperature and salinity are simply prognostic variables, and the hydrostatic pressure at a grid point varies minimally with time. By contrast, in models that use a Lagrangian vertical coordinate, the hydrostatic pressure of a grid point can vary substantially with time as a result of the ocean circulation. Sun et al. (1999) present a method for using the full nonlinear equation of state in isopycnic coordinate ocean models. They propose extracting the portion of compressibility that is a function of pressure only from the calculations of pressure gradient accelerations. This technique has proven to be useful, but it is illustrated here that an inexact compensation for compressibility in the calculation of accelerations due to pressure gradients can lead to a numerical instability that is unique to weakly stratified regions of Lagrangian vertical coordinate ocean models.

In essence, an imperfect compensation for compressibility leads to pressure gradient errors. These are equivalent to the well-known pressure gradient errors in sigma-coordinate ocean models, although usually of much smaller magnitude. In sigma-coordinate models, these lead to finite steady circulations in an ocean that is initially at rest, but are not a source of unbounded growth (e.g., Mellor and Wang, 1996). With a Lagrangian vertical coordinate, the pressure gradient errors can cause the coordinate interfaces in weakly stratified regions to migrate in a way that amplifies the pressure gradient errors, leading to an exponentially growing instability.

The consequences of this instability are readily evident in the five-day average sea surface height fields shown in Fig. 1. The two panels differ only in the treatment of compressibility in the calculation of the pressure gradient accelerations. The source of the instability lies in the very warm and weakly stratified abyssal Mediterranean; the abyssal velocities in the top case are very noisy and tens of cm s^{-1} , compared with smooth velocities of order mm s^{-1} in the lower case. This instability also shows up very clearly in the isopycnal surfaces, as seen in Fig. 2. With any globally uniform compressibility profile, this instability will occur in either the weakly stratified and cold Arctic and Antarctic waters or in the weakly stratified but warm Mediterranean. As will be discussed later, this instability can be avoided by using a spatially variable reference compressibility that closely follows the actual compressibility, while alternate discretizations of the pressure gradient terms can greatly increase the tolerance to discrepancies between the reference and actual compressibilities.

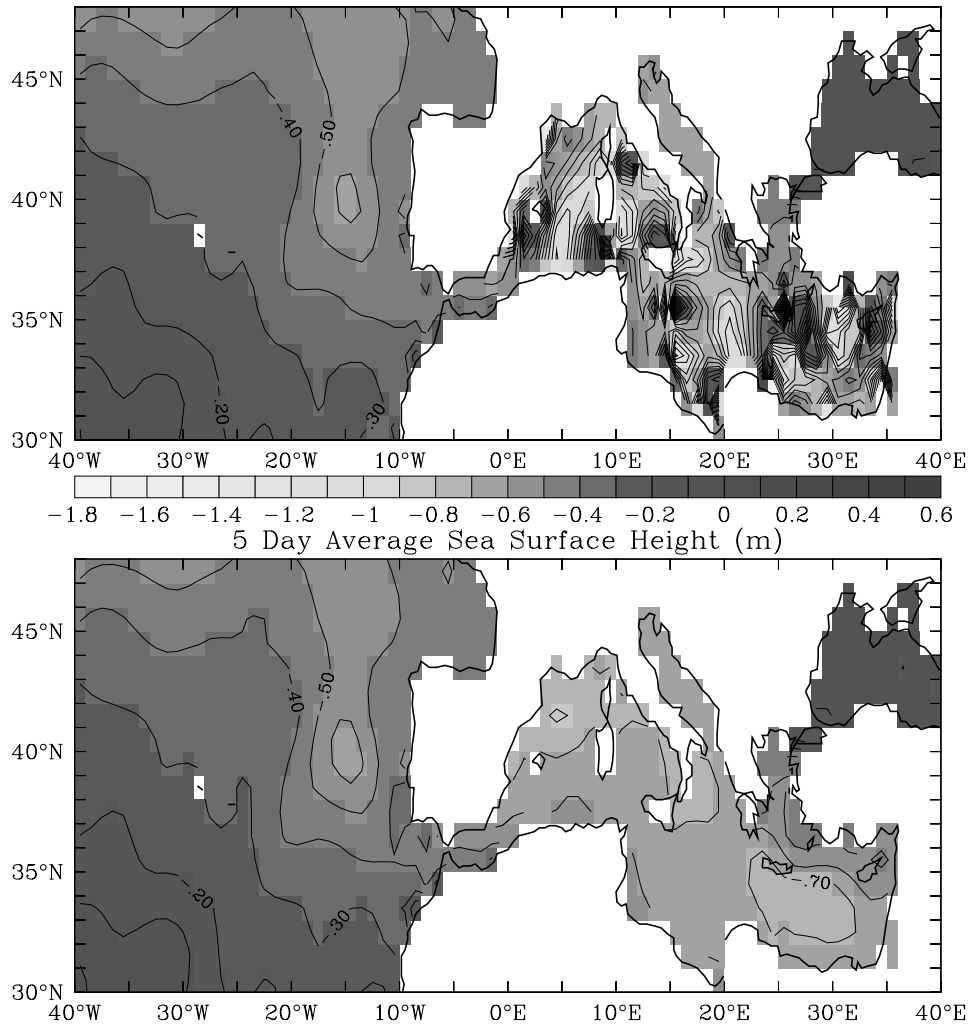


Fig. 1. Five day average sea surface height of a 48-layer 1-degree resolution global isopycnic coordinate model after 20 days. The two panels differ only in their treatment of compressibility – the top panel uses a compressibility that is typical of the Weddell Sea [and essentially the same as proposed by Sun et al. (1999)], while the bottom panel uses a horizontally variable fit to the observed compressibility and the optimal discretization of compressibility in the pressure gradient calculation (described later). Both panels use a contour interval of 10 cm.

This instability can be illustrated easily in a simple two-layer system. Analysis of this system shows that compressibility must be compensated accurately relative to the stratification to avoid instability, and that stability can be enhanced by using an optimal alternate pressure gradient discretization. This two-layer system represents any two layers of an isopycnic coordinate model, and the results can be applied directly to a system with an arbitrarily large number of layers.

It is found that the instability described here can be avoided in Lagrangian coordinate simulations of the current ocean state, while still using the full nonlinear equation of state of seawater, by extracting a compressibility that slowly varies horizontally from the density used in the pressure gradient calculations and by using a pressure gradient discretization that minimizes the impact of inexact extraction of compressibility.

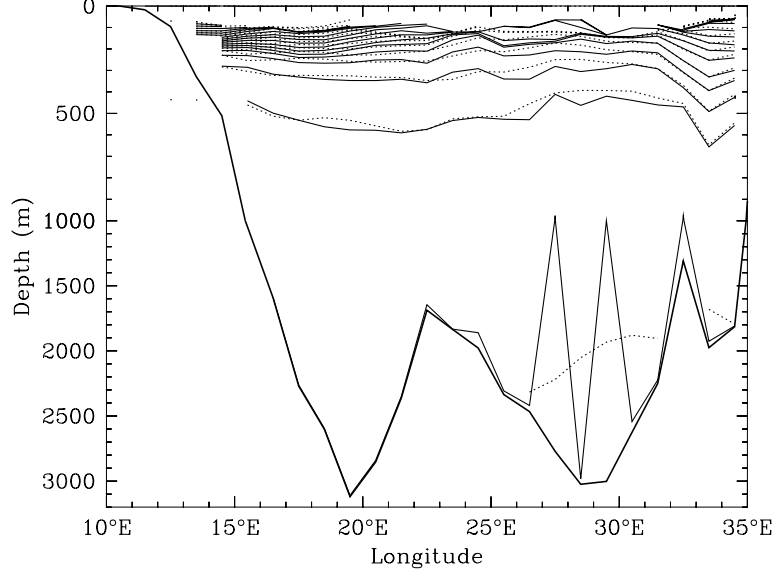


Fig. 2. Five-day average interface heights in the eastern Mediterranean along 33.5 N after 20 days for the same two simulations shown in Fig. 1. The solid lines use the compressibility that is typical of the Weddell Sea, while the dotted line uses a horizontally variable reference compressibility. Note the large excursions of the abyssal and thermocline interface heights that only occur with an inappropriate reference compressibility. Note also that in the western subbasin where the chosen target density surfaces provides no resolution of the abyssal structure, the thermocline interfaces do not show the abrupt excursions, even when the reference compressibility from the Weddell Sea is used.

2. Pressure gradient calculations in isopycnic models

Isopycnic-coordinate ocean models are a specific instance of Lagrangian vertical coordinate models, in which the vertical coordinate tracks a potential density surface. Isopycnic-coordinate ocean models have been extensively used because of their unique ability to capture the nearly adiabatic nature of the ocean interior (Bleck, 1998), their ability to represent dynamically interesting flows with relatively few degrees of freedom (e.g. Hallberg and Gnanadesikan, 2001), and the very transparent form in which potential vorticity dynamics appear in the model equations (e.g. Hallberg and Rhines, 1996 or Williams and Roussenov, 2003). Although the thermobaric instability is described here in the context of isopycnic models, it is generic to any ocean model in which the circulation substantially determines the hydrostatic pressure (as opposed to the much smaller dynamically active residual) of the grid points.

If the horizontal pressure accelerations can be cast as the gradients along the coordinate surfaces of a scalar field, the discrete form of the equations tends to have better conservation of discrete analogs of energy and potential vorticity. Such a non-solenoidal form of the hydrostatic pressure gradient accelerations can be found whenever the vertical coordinate is a function of pressure and in situ density only (deSzoek et al., 2000).

$$\alpha \nabla_{\phi} p = \nabla_p \phi = \nabla_s \phi + \alpha \nabla_s p = \nabla_s (\phi + \alpha p) - p \nabla_s \alpha = \nabla_{\alpha} (\phi + \alpha p)$$

Here α is the in situ specific volume (the inverse of density), p is pressure, $\phi = g(z - z_{\text{Ref}})$ is the geopotential, and s is an arbitrary vertical coordinate. The subscripts on the grads indicate the

surfaces along which horizontal gradients are taken. Unfortunately, there is no materially conserved function of pressure and in situ density only for the real equation of state of seawater.

To avoid solenoidal pressure gradient discretization errors, isopycnic models have traditionally simply approximated the equations of motion as if the equation of state were that of some potential density and ignored compressibility altogether (e.g. Oberhuber, 1993). The circulation errors that result from this approximation can be unacceptably large (Sun et al., 1999; deSzoek, 2000).

Sun et al. (1999) propose that the full effects of the nonlinear equation of state can be included with little algorithmic modification to existing isopycnic models by changing specific volume and geopotential variables to closely related variables that compensate for compressibility. Similar results can be derived more simply by defining a compressibility-compensated specific volume (α^*) and a corresponding counterpart of pressure (p^*) as:

$$\alpha^* = \alpha(\theta, S, p) / F'(p) \quad \text{and} \quad p^* = F(p) \quad (1)$$

where $F(p)$ is a function of pressure that remains to be determined. The compressibility-compensation will be achieved if $F(p)$ is chosen so that α^* is nearly constant in regions of constant potential temperature and salinity. The definitions (1) ensure that

$$\alpha^* \nabla_s p^* = \frac{\alpha}{F'(p)} \nabla_s F(p) = \frac{\alpha}{F'(p)} F'(p) \nabla_s p = \alpha \nabla_s p .$$

Using the hydrostatic equations

$$\frac{\partial \phi}{\partial p} = -\alpha \quad \text{and} \quad \frac{\partial \phi}{\partial p^*} = -\alpha^* , \quad (2)$$

where ϕ is geopotential, the horizontal pressure gradient acceleration becomes

$$\nabla_p \phi = \nabla_s \phi - \frac{\partial \phi}{\partial p} \nabla_s p = \nabla_s \phi + \alpha \nabla_s p = \nabla_s \phi + \alpha^* \nabla_s p^* = \nabla_s (\phi + \alpha^* p^*) - p^* \nabla_s \alpha^* . \quad (3)$$

In (3) the subscript s denotes horizontal gradients taken along surfaces of an unspecified, monotonic-with-depth quantity s . In common isopycnic modeling practice, s might be potential density referenced to 2000 dbar pressure (e.g. Sun and Bleck, 2001).

Eq. (3) can be simplified to

$$\nabla_p \phi = \nabla_s M^* - p^* \nabla_s \alpha^* . \quad (4)$$

by using a compressibility-compensated Montgomery potential

$$M^* = \phi + p^* \alpha^* . \quad (5)$$

The compensated Montgomery potential can be calculated from a differential equation with exactly the form of the traditional, uncompensated Montgomery potential, as is seen by using the hydrostatic equation (2) in the derivative of (5) with α^* :

$$\frac{\partial M^*}{\partial \alpha^*} = p^* . \quad (6)$$

The function $F(p)$ is completely arbitrary at this point. Ideally, α^* is nearly independent of pressure in the absence of changes in potential temperature or salinity. This can be accomplished by choosing $F(p)$ such that

$$\left. \frac{\partial \alpha^*}{\partial p} \right|_{\theta, S} = \frac{1}{F'(p)} \left. \frac{\partial \alpha}{\partial p} \right|_{\theta, S} - \frac{\alpha}{F'^2} \frac{dF'}{dp} \approx 0 \quad \text{or} \quad (7)$$

$$\frac{1}{F'(p)} \frac{dF'}{dp} \approx \frac{1}{\alpha} \left. \frac{\partial \alpha}{\partial p} \right|_{\theta, S}. \quad (8)$$

The interpretation of these equations is greatly simplified if the scaling of F is chosen so that $p^* \approx p$. When compressibility is compensated over the depth of the ocean, $F'(p) \approx 1$ to within about 3%, so it is possible to set $p^* \approx p$ to within about 1.5%. To the extent that $F'(p)$ satisfies (8), the compressibility effects in the solenoidal term of (4) are minimized. But since F is a function only of pressure, there is discretion in deciding which compressibility profile to fit. For example, Sun et al. (1999) use a profile with a constant salinity of 35 psu and a potential temperature of 0°C. The specific choice of a compressibility profile will be shown to have a great impact on whether the discrete flow is in fact subject to thermobaric instabilities.

3. Thermobaric Instability in a Discrete Two-layer Example

The thermobaric numerical instability is most easily illustrated with a two-layer case (Fig. 3.), where the potential temperature and salinity in each layer are constant. There are no dynamically active density anomalies within the two layers, but the dynamically inert background density varies with pressure due to compressibility. The solutions closely follow the familiar calculation of internal gravity wave frequencies (e.g. Gill, 1982). As such, the growth rates can be simply quoted once the pressure gradient differences between the two layers are determined. This two-layer example represents any two layers of an isopycnic coordinate model. The conditions that lead to the instability are identical if there are many layers, although the growth rates of the instability may be larger if there are more layers involved.

The stability of the discrete system will be determined by calculating the differences between the pressure-driven accelerations of the two layers. The system is assumed to be unstable when these accelerations tend to reinforce perturbations to the depth of the interface between the two layers, but neglected terms such as rotation or dissipation could balance these tendencies. Comparison with the vertically continuous two-layer system will reveal that these instabilities are entirely due to vertical discrete truncation errors.

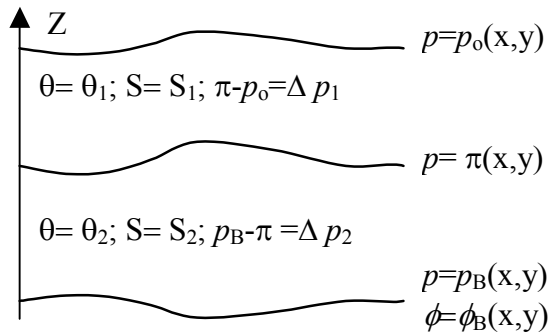


Fig. 3. Schematic side view diagram of variables in two-layer calculation.

a. *The continuous solution with two layers*

The continuous pressure gradient forces in the two-layer system are instructive to calculate for several reasons. First, it is possible to directly calculate the differences in the accelerations both using the gradient of geopotential along pressure surfaces, and via the Montgomery potential; both are included for the benefit of a reader who may be more comfortable with one form or the other. The steps in calculating the Montgomery potential form are essentially identical to those used in the discrete version, and both the final form and the intermediate steps will prove useful for comparison with the corresponding discrete expressions.

In this two-layer case, the specific volume profiles in the layers are given by:

$$\alpha_1 = A_1(p) = \alpha(\theta_1, S_1, p) , \quad (9)$$

$$\alpha_2 = A_2(p) = \alpha(\theta_2, S_2, p) \approx \alpha(\theta_1, S_1, p) - \Delta\alpha^D = A_1(p) - \Delta\alpha^D , \quad (10)$$

where θ_1 and θ_2 and S_1 and S_2 are the constant potential temperatures and salinities of the two layers. The layers are separated by an interface at pressure $p = \pi(x, y)$. These variables are depicted schematically in Fig. 3. The dynamically active specific volume difference between layers is constant and given by $\Delta\alpha^D = \alpha(\theta_1, S_1, \bar{\pi}) - \alpha(\theta_2, S_2, \bar{\pi})$, where $\bar{\pi}$ is the average value of π . The actual specific volume difference between the layers at pressure π is not constant, but for sufficiently small perturbations to the interface pressure that $|\pi - \bar{\pi}| \ll \min(\Delta p_1, \Delta p_2)$, it can be approximated as $\Delta\alpha^D$ with a smaller error than the other approximations that will be made here. In equations,

$$A_1(\pi) - A_2(\pi) = \Delta\alpha^D + (\pi - \bar{\pi}) \left(\left. \frac{\partial\alpha}{\partial p} \right|_{\theta=\theta_1, S=S_1, p=\pi} - \left. \frac{\partial\alpha}{\partial p} \right|_{\theta=\theta_2, S=S_2, p=\pi} \right) + O((\pi - \bar{\pi})^2) \approx \Delta\alpha^D .$$

Henceforth this small amplitude approximation will be made without comment.

Starting at the bottom of the lower layer, the continuous geopotentials in the two layers are readily calculated from the hydrostatic equation (2):

$$\phi_2(p) = \phi_B - \int_{p_B}^p A_2(\tilde{p}) d\tilde{p} , \quad (11)$$

$$\phi_1(p) = \phi_B - \int_{p_B}^{\pi} A_2(\tilde{p}) d\tilde{p} - \int_{\pi}^p A_1(\tilde{p}) d\tilde{p} . \quad (12)$$

The difference in the horizontal pressure gradient accelerations between the two layers is

$$\begin{aligned} \nabla_p \phi_1 - \nabla_p \phi_2 &= [\nabla \phi_B + A_2(p_B) \nabla p_B - A_2(\pi) \nabla \pi + A_1(\pi) \nabla \pi] - [\nabla \phi_B + A_2(p_B) \nabla p_B] \\ &= [A_1(\pi) - A_2(\pi)] \nabla \pi \\ &\approx \Delta\alpha^D \nabla \pi \end{aligned} \quad (13)$$

In the non-rotating case, displacements to the internal interface propagate away as internal gravity waves with speed

$$c_{int} \approx \sqrt{\Delta\alpha^D \Delta p_1 \Delta p_2 / (\Delta p_1 + \Delta p_2)} \quad (14)$$

(e.g. Gill (1982), section 6.2), where $\Delta p_1 = \pi - p_o$ and $\Delta p_2 = p_B - \pi$ are the pressure thicknesses of the two layers, as shown in Fig. 3.

For later comparison with the discrete calculations, it is useful to calculate the horizontal pressure gradient accelerations in the two layers again using the Montgomery potential form, (4).

Integrating the differential equation for the Montgomery potential (6) upward, the Montgomery potentials of the two layers are

$$\begin{aligned}
\nabla_s M_2^* &= \nabla_s (\phi_2 + \alpha_2^* p^*) \\
&= \nabla_s \left[\phi_2 + \frac{A_2(p)}{F'(p)} F(p) \right] \\
&= \nabla \phi_B + A_2 \nabla p_B - A_2(p) \nabla_s p + \frac{A_2(p) F'(p)}{F'(p)} \nabla_s p + F(p) \nabla_s \frac{A_2(p)}{F'(p)} \\
&= \nabla \phi_B + A_2 \nabla p_B + p^* \nabla_s \alpha_2^*
\end{aligned} \tag{15}$$

$$\begin{aligned}
\nabla_s M_1^* &= \nabla_s (\phi_1 + \alpha_1^* p^*) \\
&= \nabla_s \left[\phi_1 + \frac{A_1(p)}{F'(p)} F(p) \right] \\
&= \nabla \phi_B + A_2 \nabla p_B - A_2(\pi) \nabla_s \pi + A_1(\pi) \nabla_s \pi - A_1(p) \nabla_s p + A_1(p) \nabla_s p + F(p) \nabla_s \frac{A_1(p)}{F'(p)} \\
&\approx \nabla \phi_B + A_2 \nabla p_B + \Delta \alpha^D \nabla_s \pi + p^* \nabla_s \alpha_1^*
\end{aligned} \tag{16}$$

The difference in the horizontal pressure gradient accelerations of the two layers must agree with (13):

$$(\nabla_s M_1^* - p^* \nabla_s \alpha_1^*) - (\nabla_s M_2^* - p^* \nabla_s \alpha_2^*) = [A_1(\pi) - A_2(\pi)] \nabla \pi \approx \Delta \alpha^D \nabla \pi . \tag{17}$$

The discrete case will later be shown to agree with (17) at leading order, but will also contain thermobaric truncation error terms.

b. *The vertically discrete solution with two layers*

When the two-layer system is vertically discretized but kept horizontally continuous, the only real discretization choice is the pressure at which to evaluate the layer specific volume, α . It is assumed that this layer specific volume is used in the hydrostatic equation, (2). In isopycnic models, it is customary to use the pressure at the top of a layer so that topography will not cause accelerations when the isopycnals are flat (Sun and Bleck, 2001). In this section this convention will be followed, although it will be shown later that the thermobaric instability still occurs if other choices are made.

The difference in the discrete pressure-force accelerations of the two layers is straightforward to calculate once the layer specific volumes are specified. Using the pressure at the top of the layer to determine the layer specific volumes gives

$$\alpha_1^* = \frac{\alpha(\theta_1, S_1, p_0)}{F'(p_0)} \quad \text{and} \quad \alpha_2^* = \frac{\alpha(\theta_2, S_2, \pi)}{F'(\pi)} . \tag{18}$$

From the differential equation for the Montgomery potential (6), the horizontal gradients of the Montgomery potential in the upper and lower layers are related by

$$\begin{aligned}
\nabla M_2^* - \nabla M_1^* &= \nabla [F(\pi) (\alpha_2^* - \alpha_1^*)] \\
&= (\alpha_2^* - \alpha_1^*) F'(\pi) \nabla \pi + F(\pi) \nabla (\alpha_2^* - \alpha_1^*)
\end{aligned} \tag{19}$$

From the Mean Value Theorem, for some pressure \tilde{p}_1 within the range of the first layer (near the mean pressure of the layer),

$$\begin{aligned}
\alpha_1^* &= \frac{\alpha(\theta_1, S_1, \pi)}{F'(\pi)} - (\pi - p_0) \frac{\partial \alpha^*}{\partial p} \Big|_{\theta=\theta_1, S=S_1, p=\tilde{p}_1} \\
&= \alpha_2^* + \frac{\Delta \alpha^D}{F'(\pi)} - \Delta p_1 \frac{\partial \alpha^*}{\partial p} \Big|_{1, \tilde{p}_1}
\end{aligned} \tag{20}$$

In the second line of (20), the subscript indicating that the partial derivative of α^* with pressure is taken at values appropriate to the upper layer has been abbreviated as $1, \tilde{p}_1$ for notational convenience. Eq. (19) can be rewritten as

$$\begin{aligned}
\nabla M_2^* - \nabla M_1^* &= \left(-\frac{\Delta \alpha^D}{F'(\pi)} + \Delta p_1 \frac{\partial \alpha^*}{\partial p} \Big|_{1, \tilde{p}_1} \right) F'(\pi) \nabla \pi + F(\pi) \nabla (\alpha_2^* - \alpha_1^*) \\
&= -\Delta \alpha^D \nabla \pi + F'(\pi) \Delta p_1 \frac{\partial \alpha^*}{\partial p} \Big|_{1, \tilde{p}_1} \nabla \pi + F(\pi) \nabla (\alpha_2^* - \alpha_1^*)
\end{aligned} \tag{21}$$

The solenoidal term that arises with the Montgomery potential form of the horizontal pressure gradient acceleration (4) typically uses the central pressure of a layer (Bleck, 2002) and the same choice of layer specific volume as in the calculation of M .¹ The solenoidal terms in the two layers become:

$$p_1^* \nabla \alpha_1^* = \frac{F(p_0) + F(\pi)}{2} \nabla \frac{\alpha(\theta_1, S_1, p_0)}{F'(p_0)} \quad \text{and} \quad p_2^* \nabla \alpha_2^* = \frac{F(\pi) + F(p_B)}{2} \nabla \frac{\alpha(\theta_2, S_2, \pi)}{F'(\pi)}. \tag{22}$$

Combining (21) and (22), the difference in the horizontal pressure gradient accelerations (4) become:

$$\begin{aligned}
\nabla M_2^* - p_2^* \nabla \alpha_2^* - \nabla M_1^* + p_1^* \nabla \alpha_1^* \\
&= -\Delta \alpha^D \nabla \pi + F'(\pi) \Delta p_1 \frac{\partial \alpha^*}{\partial p} \Big|_{1, \tilde{p}_1} \nabla \pi + \frac{F(\pi) - F(p_B)}{2} \nabla \alpha_2^* - \frac{F(\pi) - F(p_0)}{2} \nabla \alpha_1^* \\
&= -\Delta \alpha^D \nabla \pi + F'(\pi) \Delta p_1 \frac{\partial \alpha^*}{\partial p} \Big|_{1, \tilde{p}_1} \nabla \pi - F'(\tilde{p}_2) \frac{\Delta p_2}{2} \frac{\partial \alpha^*}{\partial p} \Big|_{2, \pi} \nabla \pi - F'(\tilde{p}_1) \frac{\Delta p_1}{2} \frac{\partial \alpha^*}{\partial p} \Big|_{1, p_0} \nabla p_0
\end{aligned} \tag{23}$$

If compressibility is well-compensated (i.e. (8) is satisfied), $F'(p) \approx 1$ to within about 3% for oceanographic conditions, so

$$\begin{aligned}
\nabla M_2^* - p_2^* \nabla \alpha_2^* - \nabla M_1^* + p_1^* \nabla \alpha_1^* \\
\approx - \left(\Delta \alpha^D - \Delta p_1 \frac{\partial \alpha^*}{\partial p} \Big|_{1, \tilde{p}_1} + \frac{\Delta p_2}{2} \frac{\partial \alpha^*}{\partial p} \Big|_{2, \pi} \right) \nabla \pi - \frac{\Delta p_1}{2} \frac{\partial \alpha^*}{\partial p} \Big|_{1, p_0} \nabla p_0
\end{aligned} \tag{24}$$

The difference between this discrete solution and the true solution, (17), is

$$Error \approx \left(\Delta p_1 \frac{\partial \alpha^*}{\partial p} \Big|_{1, \tilde{p}_1} - \frac{\Delta p_2}{2} \frac{\partial \alpha^*}{\partial p} \Big|_{2, \pi} \right) \nabla \pi - \frac{\Delta p_1}{2} \frac{\partial \alpha^*}{\partial p} \Big|_{1, p_0} \nabla p_0, \tag{25}$$

¹The Montgomery potential-based form of the pressure gradient terms described by Bleck (2002), and in long-standing use in isopycnal models, is mathematically identical to the Jacobian form advocated by Lin (1997), once the density profiles are chosen to be vertically constant within a layer.

so this is a first order discrete truncation error in layer thickness, as is consistent with the formal order of accuracy in the choice of α in the layers.

The last term in (24) is irrelevant for the purposes of evaluating the linear stability of the two-layer system to perturbations of the internal interface height, as it provides no direct feedback of perturbations to π on the flow. Substituting the entire term in parentheses in (24) for $\Delta\alpha^D$ in the internal wave dispersion relation (14) shows that the flow in these two layers is unstable at all horizontal wavelengths if

$$\Delta\alpha^D - \Delta p_1 \left. \frac{\partial\alpha^*}{\partial p} \right|_{1,\tilde{p}_1} + \frac{\Delta p_2}{2} \left. \frac{\partial\alpha^*}{\partial p} \right|_{2,\pi} < 0 . \quad (26)$$

In a non-rotating two-layer system, the growth of perturbations with horizontal wavenumber k is given by

$$\frac{\partial\pi}{\partial t} = \exp(\lambda t) . \quad (27)$$

where

$$\lambda \approx k \sqrt{-\frac{\Delta p_1 \Delta p_2}{\Delta p_1 + \Delta p_2} \left(\Delta\alpha^D - \Delta p_1 \left. \frac{\partial\alpha^*}{\partial p} \right|_{1,\tilde{p}_1} + \frac{\Delta p_2}{2} \left. \frac{\partial\alpha^*}{\partial p} \right|_{2,\pi} \right)} . \quad (28)$$

The mathematics behind this statement are identical to the calculation of the two-layer internal gravity wave dispersion relation (e.g. Gill, 1982). The growth rates here may be comparable to the frequencies of high mode internal gravity waves. Refining the vertical resolution of a model will tend to simultaneously reduce $\Delta\alpha^D$ and Δp_n proportionally, so while it may reduce the growth rates, the conditions for instability (26) are essentially independent of vertical resolution. The sole controllable consideration in whether a Lagrangian vertical coordinate ocean model is subject to this instability is the relative accuracy of the thermobaric compensation to the stratification of the ocean.

There are two distinct manifestations of the pressure gradient truncation errors that lead to the condition (26) for instability being satisfied; these are illustrated in Fig. 4. If the instability is satisfied because

$$\Delta\alpha^D - \Delta p_1 \left. \frac{\partial\alpha^*}{\partial p} \right|_{1,\tilde{p}_1} < 0 \quad (29)$$

(illustrated in Fig. 4. b.), there will appear to be a negative apparent reduced gravity across the interface (i.e. $\alpha_2^* > \alpha_1^*$), leading to changes in M^* between layers from (6) that depend on the interface pressure with the opposite of the usual sign. On the other hand, if the instability occurs predominantly because

$$\Delta\alpha^D + \frac{\Delta p_2}{2} \left. \frac{\partial\alpha^*}{\partial p} \right|_{2,\pi} < 0 \quad (30)$$

(illustrated in Fig. 4. c.), the layer below an interface that is displaced upward appears to become lighter and the non-solenoidal term (i.e. $-p^* \nabla \alpha^*$) acts to reinforce this displacement; the hydrostatic pressure forces generated within a layer are toward lighter fluid. Instability occurs when the sensitivity of the non-solenoidal term to the interface depth overwhelms the restoring

tendency in the gradient of the Montgomery potential. The former instability occurs at the base of thick layers in waters that are much warmer than the reference profile upon which the compensating compressibility is based. The latter manifestation occurs at the top of thick layers that are much colder than the reference profile.

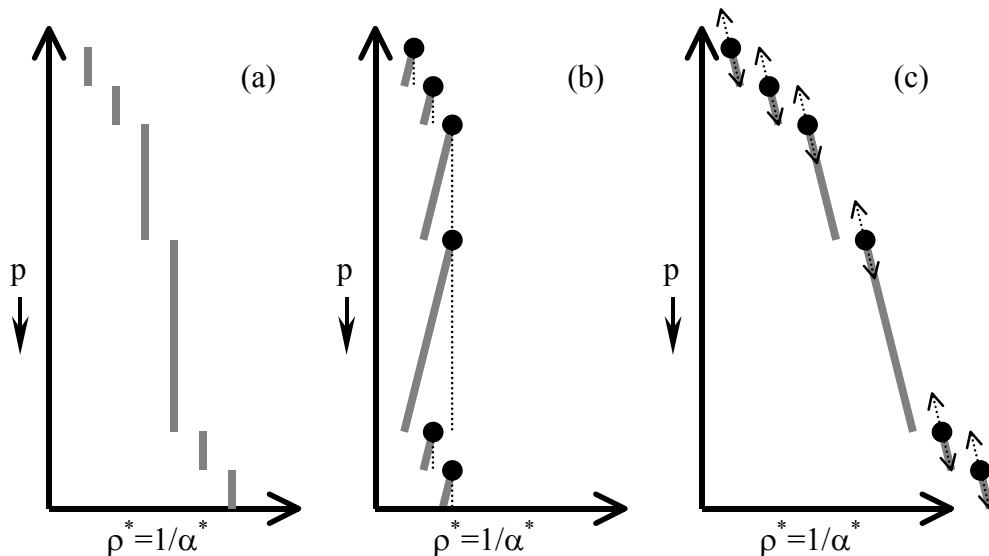


Fig. 4. Profiles of α^* in layers of constant potential temperature and salinity in instances where (a) compressibility is perfectly compensated, (b) compressibility is over-compensated (i.e. a colder profile is used to determine the reference compressibility), and (c) the compressibility is under- or un-compensated. The circles in (b) and (c) and the dotted line in (b) show the assumed values for the whole layer when α^* is evaluated at the top of each layer. The lines and arrows in (c) indicate how α^* changes when the interface atop the layer moves – this occurs in the cases sketched in both (b) and (c), but it is in case (c) that these changes are destabilizing.

4. Physical conditions for instability

The stratification of the ocean itself determines how prone a Lagrangian vertical coordinate model will be to thermobaric instability. The buoyancy frequency can be expressed as

$$N^2 = -\frac{g^2}{\alpha^2} \left(\frac{d\alpha}{dp} - \frac{\partial\alpha}{\partial p} \Big|_{\theta,S} \right) \approx \frac{g^2}{\alpha^2} \frac{\Delta\alpha^D}{\Delta p} . \quad (31)$$

The Δp in (31) would be some appropriate (undetermined) average of Δp_1 and Δp_2 in the two-layer example. This interpretation is most accurate in the limit of fine vertical resolution. The two-layer instability condition, (26), can be reinterpreted as a constraint on how well compressibility must be compensated, relative to the stratification, to avoid the instability. Assuming that the sign of the errors in the compressibility does not change in adjacent layers where the errors themselves are large, stability is ensured if

$$-2 \frac{\alpha}{g^2} N^2 < \frac{1}{\alpha^*} \frac{\partial\alpha^*}{\partial p} \Big|_{\theta,S} = \left(\frac{1}{\alpha} \frac{\partial\alpha}{\partial p} \Big|_{\theta,S} - \frac{1}{F'} \frac{\partial F'}{\partial p} \right) < \frac{\alpha}{g^2} N^2 . \quad (32)$$

Introducing the sound speed, c_s , given by

$$c_s^{-2} = -\frac{1}{\alpha^2} \left. \frac{\partial \alpha}{\partial p} \right|_{\theta, S}, \quad (33)$$

instability will be avoided if

$$-\frac{\alpha}{g^2} N^2 < \alpha c_s^{-2} + \frac{1}{F'} \frac{\partial F'}{\partial p} < 2 \frac{\alpha}{g^2} N^2. \quad (34)$$

In the NODC 1998 ocean atlas (Levitus et al., 1998), there are many areas of the ocean with stratifications weak enough that $N^2 \approx 2 \times 10^{-7} \text{ s}^{-2}$ over vertical scales of hundreds of meters. Notably, this value is typical of both the Weddell Sea and the Mediterranean Sea at depths of 1-3 km. But the temperatures and salinities of the two areas are very different - the Mediterranean is about 13 K warmer and 3.7 psu saltier than the Weddell Sea at these depths – implying very different compressibilities. As seen in Fig. 5. , the compressibility of sea water, αc_s^{-2} , varies with temperature and salinity at rates of order $\frac{\partial}{\partial \theta}(\alpha c_s^{-2}) \approx -2.3 \times 10^{-12} \text{ Pa}^{-1} \text{ K}^{-1}$ and

$\frac{\partial}{\partial S}(\alpha c_s^{-2}) \approx -1.1 \times 10^{-12} \text{ Pa}^{-1} \text{ psu}^{-1}$, compared with its mean value of order $4.5 \times 10^{-10} \text{ Pa}^{-1}$. To satisfy (34) in water with $N^2 \approx 2 \times 10^{-7} \text{ s}^{-2}$, the compressibility must be characteristic of water that is no more than 1.8 K warmer or 0.9 K colder than is actually found (assuming the right salinity) and no more than 4.2 psu saltier or 2.1 psu fresher (now assuming the right temperature). Clearly there is no single reference compressibility profile that will avoid the thermobaric numerical instability for both the Weddell Sea and the Mediterranean.

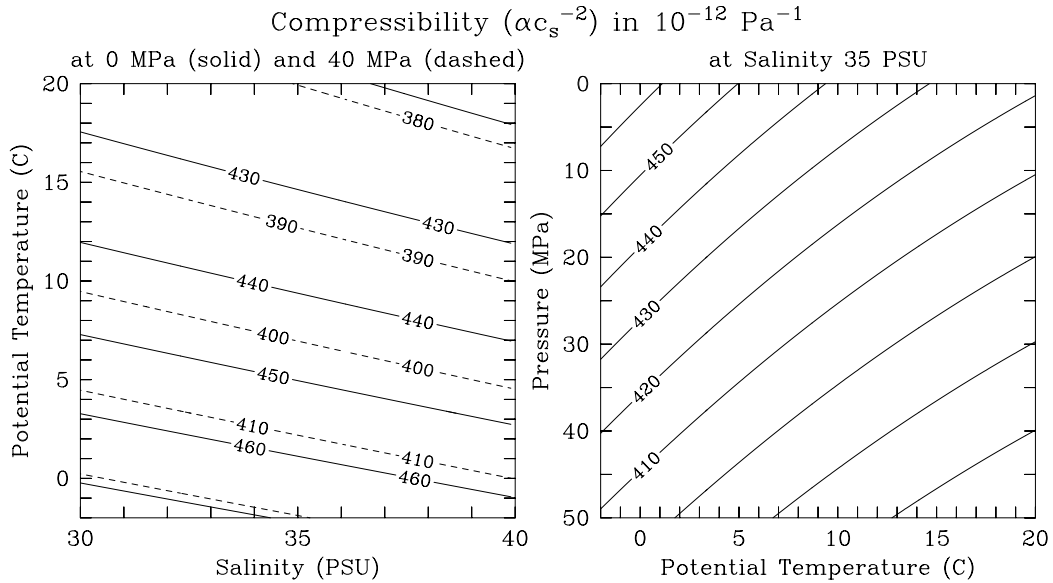


Fig. 5. The compressibility of seawater in 10^{-12} Pa^{-1} as a function of salinity and potential temperature (left) at pressures of 0 (solid) and 40 MPa (dashed) and as a function of potential temperature and pressure (right) at a salinity of 35 PSU. The contour interval is $10 \times 10^{-12} \text{ Pa}^{-1}$ in both cases.

5. Alternate discrete forms

Returning to the two-layer example, there are three other discrete forms that are worth considering. As the derivation is essentially the same as in section 3, the pertinent results will simply be quoted. In each case the thermobaric instability is still present, but with a greater tolerance for inaccuracy in the compensation of compressibility. The first two alternatives are obvious possibilities – taking the layer average specific volume or the layer average Montgomery potential. These can be combined to give an optimal form that eliminates the thermobaric error terms to leading order.

First, suppose that the compensated layer specific volume is taken as the average of the values at the top and bottom of a layer. Then the equivalent of (18) is

$$\bar{\alpha}_1^* = \frac{1}{2} \left[\frac{\alpha(\theta_1, S_1, p_0)}{F'(p_0)} + \frac{\alpha(\theta_1, S_1, \pi)}{F'(\pi)} \right] \text{ and } \bar{\alpha}_2^* = \frac{1}{2} \left[\frac{\alpha(\theta_2, S_2, \pi)}{F'(\pi)} + \frac{\alpha(\theta_2, S_2, p_B)}{F'(p_B)} \right], \quad (35)$$

while the counterpart of (20) is

$$\bar{\alpha}_1^* - \bar{\alpha}_2^* = \frac{\Delta\alpha^D}{F'(\pi)} - \frac{\Delta p_1}{2} \frac{\partial \alpha^*}{\partial p} \Big|_{1, \tilde{p}_1} - \frac{\Delta p_2}{2} \frac{\partial \alpha^*}{\partial p} \Big|_{2, \tilde{p}_2}. \quad (36)$$

The difference in the horizontal pressure gradient accelerations (corresponding to (23)) with this first alternate discretization is

$$\begin{aligned} & \nabla \hat{M}_2^* - \bar{p}_2^* \nabla \bar{\alpha}_2^* - \nabla \hat{M}_1^* + \bar{p}_1^* \nabla \bar{\alpha}_1^* \\ &= -\Delta\alpha^D \nabla \pi + F'(\pi) \frac{\Delta p_1}{2} \frac{\partial \alpha^*}{\partial p} \Big|_{1, \tilde{p}_1} \nabla \pi + F'(\pi) \frac{\Delta p_2}{2} \frac{\partial \alpha^*}{\partial p} \Big|_{1, \tilde{p}_2} \nabla \pi - F'(\tilde{p}_2) \frac{\Delta p_2}{4} \frac{\partial \alpha^*}{\partial p} \Big|_{2, \pi} \nabla \pi \\ & \quad - F'(\tilde{p}_1) \frac{\Delta p_1}{4} \frac{\partial \alpha^*}{\partial p} \Big|_{1, \pi} \nabla \pi - F'(\tilde{p}_2) \frac{\Delta p_2}{4} \frac{\partial \alpha^*}{\partial p} \Big|_{2, p_B} \nabla p_B - F'(\tilde{p}_1) \frac{\Delta p_1}{4} \frac{\partial \alpha^*}{\partial p} \Big|_{1, p_0} \nabla p_0. \quad (37) \\ & \approx - \left(\Delta\alpha^D - \frac{\Delta p_1}{4} \frac{\partial \alpha^*}{\partial p} \Big|_1 - \frac{\Delta p_2}{4} \frac{\partial \alpha^*}{\partial p} \Big|_2 \right) \nabla \pi - \frac{\Delta p_1}{4} \frac{\partial \alpha^*}{\partial p} \Big|_1 \nabla p_0 - \frac{\Delta p_2}{4} \frac{\partial \alpha^*}{\partial p} \Big|_2 \nabla p_B \end{aligned}$$

The approximations leading to the final line of (37) are that the mismatches between the true compressibility and the reference compressibility are roughly constant within a layer and that $F'(p) \approx 1$ [as was assumed in deriving (24)]. This alternative is intriguing, both because the thresholds for instability are easier to avoid by a factor of 2 or 4, and because the thermodynamic instability itself can be avoided by choosing $F(p)$ such that $\partial \alpha^* / \partial p < 0$ wherever the stratification is weak. (Underestimating the compressibility is the equivalent of choosing a warm reference profile.) This form gives formal second order accuracy, as should be expected from a centered discretization, but as with the previous scheme, the necessary conditions for stability (i.e. the accuracy with which the reference compressibility must approximate the actual compressibility for a given stratification) do not change with increasing resolution.

Unfortunately, there is a significant price to be paid for using this form in that the bottom pressure gradients induce shears between the two layers. Since the bottom pressure gradients are usually dominated by topography, using this form leads to a model that does not sit quiescently when all of the interior isopycnals are flat. In the limit where the dynamically active density

gradients in (37) are much larger than the spurious compressibility terms, the internal interface shape that does not drive acceleration of a shear is approximately given by

$$\nabla \pi \approx \frac{-\frac{\Delta p_2}{4} \frac{\partial \alpha^*}{\partial p} \Big|_2}{\Delta \alpha^D - \frac{\Delta p_1}{4} \frac{\partial \alpha^*}{\partial p} \Big|_1 - \frac{\Delta p_2}{4} \frac{\partial \alpha^*}{\partial p} \Big|_2} \nabla p_B . \quad (38)$$

Unless the compressibility is extremely well compensated in α^* , the internal interfaces far above topography may unphysically reflect the bottom topography where the near bottom stratification is quite weak. In addition, if interface height diffusion is used as an eddy or numerical closure, the interface will not match the resting depth (38) and there will be an unphysical flow around topography.

If the layer specific volumes are evaluated at the mean pressure of the layers, the results are equivalent to the previous case, except that the pressures at which $\partial \alpha^*/\partial p$ is evaluated in (37) are different.

Another alternative that is worth considering is to assume that the α^* within each layer vary linearly with p^* , and to calculate the average compensated Montgomery potentials of the layers accordingly. From the hydrostatic equation in the form (6), if the pressure at the top and bottom of layer N are p_N^T and p_N^B , then using the definitions

$$\alpha_N^{*T} = \frac{\alpha(\theta_N, S_N, p_N^T)}{F'(p_N^T)}, \quad \alpha_N^{*B} = \frac{\alpha(\theta_N, S_N, p_N^B)}{F'(p_N^B)}, \quad p_N^{*T} = F(p_N^T), \quad \text{and} \quad p_N^{*B} = F(p_N^B), \quad (39)$$

the relationship between the Montgomery potentials at the layer's top and bottom (denoted by superscripts T and B) and its average over a layer are

$$\overline{M}_N^* - M_N^{*T} = \frac{1}{6} (\alpha_N^{*B} - \alpha_N^{*T}) (2p_N^{*T} + p_N^{*B}) \quad (40)$$

$$M_N^{*B} - \overline{M}_N^* = \frac{1}{6} (\alpha_N^{*B} - \alpha_N^{*T}) (p_N^{*T} + 2p_N^{*B}). \quad (41)$$

These can be combined with the Montgomery potential jump between layers given by (6),

$$M_{N+1}^{*T} - M_N^{*B} = (\alpha_{N+1}^{*T} - \alpha_N^{*B}) p_N^{*B} \equiv (\alpha_{N+1}^{*T} - \alpha_N^{*B}) p_{N+1}^{*T}, \quad (42)$$

to give the relationship between the Montgomery potentials averaged over the two layers:

$$\begin{aligned} \overline{M}_2^* - \overline{M}_1^* &= (\alpha_2^{*T} - \alpha_1^{*B}) p_1^{*B} + \frac{1}{6} (\alpha_1^{*B} - \alpha_1^{*T}) (p_1^{*T} + 2p_1^{*B}) + \frac{1}{6} (\alpha_2^{*B} - \alpha_2^{*T}) (2p_2^{*T} + p_2^{*B}) \\ &= -\frac{\Delta \alpha^D}{F'(\pi)} F(\pi) + \frac{1}{6} (\alpha_1^{*B} - \alpha_1^{*T}) (F(p_o) + 2F(\pi)) + \frac{1}{6} (\alpha_2^{*B} - \alpha_2^{*T}) (2F(\pi) + F(p_B)) \end{aligned} \quad (43)$$

Eq. (43) is useful for analyzing the stability of this discrete form. A rearrangement of the first line of (43) gives an alternate form of the same expression that will guide the discretization of \overline{M}_N^* :

$$\overline{M}_2^* - \overline{M}_1^* = (\alpha_2^* - \alpha_1^*) p_1^{*B} - \frac{1}{6} (\alpha_1^{*B} - \alpha_1^{*T}) (p_1^{*B} - p_1^{*T}) + \frac{1}{6} (\alpha_2^{*B} - \alpha_2^{*T}) (p_2^{*B} - p_2^{*T}). \quad (44)$$

The difference in the horizontal pressure gradient accelerations (corresponding to (23)) with this discretization is:

$$\begin{aligned}
& \nabla \bar{M}_2^* - \bar{p}_2^* \nabla \bar{\alpha}_2^* - \nabla \bar{M}_1^* + \bar{p}_1^* \nabla \bar{\alpha}_1^* \\
& = -\Delta \alpha^D \nabla \pi + F'(\pi) \left. \frac{\Delta p_1}{3} \frac{\partial \alpha^*}{\partial p} \right|_{1, \tilde{p}_1} \nabla \pi + F'(\pi) \left. \frac{\Delta p_2}{3} \frac{\partial \alpha^*}{\partial p} \right|_{1, \tilde{p}_2} \nabla \pi \\
& \quad + F'(p_o) \left. \frac{\Delta p_1}{6} \frac{\partial \alpha^*}{\partial p} \right|_{1, \tilde{p}_1} \nabla p_o + F'(p_B) \left. \frac{\Delta p_2}{6} \frac{\partial \alpha^*}{\partial p} \right|_{2, \tilde{p}_2} \nabla p_B - F'(\tilde{p}_1) \left. \frac{5 \Delta p_1}{12} \frac{\partial \alpha^*}{\partial p} \right|_{1, \pi} \nabla \pi \quad . \\
& \quad - F'(\tilde{p}_2) \left. \frac{5 \Delta p_2}{12} \frac{\partial \alpha^*}{\partial p} \right|_{2, \pi} \nabla \pi - F'(\tilde{p}_1) \left. \frac{\Delta p_1}{12} \frac{\partial \alpha^*}{\partial p} \right|_{1, p_o} \nabla p_o - F'(\tilde{p}_2) \left. \frac{\Delta p_2}{12} \frac{\partial \alpha^*}{\partial p} \right|_{2, p_B} \nabla p_B \\
& \approx - \left(\Delta \alpha^D + \left. \frac{\Delta p_1}{12} \frac{\partial \alpha^*}{\partial p} \right|_1 + \left. \frac{\Delta p_2}{12} \frac{\partial \alpha^*}{\partial p} \right|_2 \right) \nabla \pi + \left. \frac{\Delta p_1}{12} \frac{\partial \alpha^*}{\partial p} \right|_1 \nabla p_o + \left. \frac{\Delta p_2}{12} \frac{\partial \alpha^*}{\partial p} \right|_2 \nabla p_B
\end{aligned} \tag{45}$$

The assumptions leading to the final line of (45) are the same as for (37). The proclivity to thermobaric instability is greatly reduced with this form of the equations, by a factor of 6 or 12 compared with evaluating the specific volumes at the top of each layer, and by a factor of 3 compared with using the central pressure of each layer to obtain a vertically constant specific volume. With this form, the instability can be avoided by overestimating compressibility (equivalent to taking a cold reference profile). While the impact of bottom pressures on the shear between layers is reduced by a factor of 3 compared with the previous alternate scheme, it is still present, along with the undesirable consequences.

Finally, it is worth noting that if the first two alternate discretizations (using a constant specific volume at the average pressure and a linearly varying specific volume) are combined in a ratio of 1:3 as $\bar{M}_N^* = \frac{3}{4} \bar{M}_N^* + \frac{1}{4} \hat{M}_N^*$, the difference in the horizontal pressure gradient accelerations becomes

$$\begin{aligned}
& \nabla \bar{M}_2^* - p_2^* \nabla \alpha_2^* - \nabla \bar{M}_1^* + p_1^* \nabla \alpha_1^* \\
& = -\Delta \alpha^D \nabla \pi + F'(\pi) \left. \frac{3 \Delta p_1}{8} \frac{\partial \alpha^*}{\partial p} \right|_{1, \tilde{p}_1} \nabla \pi + F'(\pi) \left. \frac{3 \Delta p_2}{8} \frac{\partial \alpha^*}{\partial p} \right|_{1, \tilde{p}_2} \nabla \pi \\
& \quad + F'(p_o) \left. \frac{\Delta p_1}{8} \frac{\partial \alpha^*}{\partial p} \right|_{1, \tilde{p}_1} \nabla p_o + F'(p_B) \left. \frac{\Delta p_2}{8} \frac{\partial \alpha^*}{\partial p} \right|_{2, \tilde{p}_2} \nabla p_B - F'(\tilde{p}_1) \left. \frac{3 \Delta p_1}{8} \frac{\partial \alpha^*}{\partial p} \right|_{1, \pi} \nabla \pi \\
& \quad - F'(\tilde{p}_2) \left. \frac{3 \Delta p_2}{8} \frac{\partial \alpha^*}{\partial p} \right|_{2, \pi} \nabla \pi - F'(\tilde{p}_1) \left. \frac{\Delta p_1}{8} \frac{\partial \alpha^*}{\partial p} \right|_{1, p_o} \nabla p_o - F'(\tilde{p}_2) \left. \frac{\Delta p_2}{8} \frac{\partial \alpha^*}{\partial p} \right|_{2, p_B} \nabla p_B \quad . \\
& = - \left\{ \Delta \alpha^D - \frac{3 \Delta p_1}{8} \left[\left. \frac{\partial \alpha^*}{\partial p} \right|_{1, \tilde{p}_1} - \left. \frac{\partial \alpha^*}{\partial p} \right|_{1, \pi} \right] - \frac{3 \Delta p_2}{8} \left[\left. \frac{\partial \alpha^*}{\partial p} \right|_{1, \tilde{p}_2} - \left. \frac{\partial \alpha^*}{\partial p} \right|_{2, \pi} \right] \right\} \nabla \pi \\
& \quad + \frac{\Delta p_1}{8} \left[\left. \frac{\partial \alpha^*}{\partial p} \right|_{1, \tilde{p}_1} - \left. \frac{\partial \alpha^*}{\partial p} \right|_{1, p_o} \right] \nabla p_o + \frac{\Delta p_2}{8} \left[\left. \frac{\partial \alpha^*}{\partial p} \right|_{1, \tilde{p}_2} - \left. \frac{\partial \alpha^*}{\partial p} \right|_{2, p_B} \right] \nabla p_B \\
& \approx -\Delta \alpha^D \nabla \pi
\end{aligned} \tag{46}$$

The final approximation in (46) is at the same level of error as the approximations in (24), (37), and (45) – namely that the $F'(p)$ and the compressibility mismatches ($\partial \alpha^* / \partial p$) are both constant through a layer. This final approximation agrees with the true solution, (17). The dependence of the pressure-driven shear on the layer structure is localized to a single interface to one higher

power in Δp than in any of the discretizations discussed previously. With this discretization the necessary conditions for instability become less restrictive as the vertical resolution is increased. Put differently, to the extent that higher resolutions in density space enable the representation of weaker stratification, this discretization is much less likely than the others to become unstable as resolution is increased.

This optimal combination can be discretized quite readily. Eq. (44) implies that the vertically averaged Montgomery potential assuming a linear specific volume profile (\bar{M}_N^*) is related to the Montgomery potential based on a constant layer-mean specific volume (\hat{M}_N^*) by:

$$\bar{M}_N^* - \hat{M}_N^* = \frac{1}{6} (\alpha_N^{*B} - \alpha_N^{*T}) (p_N^{*B} - p_N^{*T}). \quad (47)$$

This potentially optimal discretization of M (\bar{M}_N^*) can then be found quite simply from

$$\tilde{M}_N^* - \hat{M}_N^* = \frac{1}{8} (\alpha_N^{*B} - \alpha_N^{*T}) (p_N^{*B} - p_N^{*T}). \quad (48)$$

In practice this scheme works quite well, provided that the local compressibility is reasonably well approximated. It is also relatively tolerant of mismatches between the reference and actual compressibility, as seen in Fig. 6.

Simulations with a 48-layer isopycnic model show the behavior predicted by the analysis of the two-layer system. Using a compressibility that is typical of the Weddell Sea, the abyssal Mediterranean is ill-behaved with all the discretizations (see Fig. 1.). If the compressibility is typical of the Mediterranean, the first alternate form exhibits strong interface excursions that reflect the topography in weakly stratified abyssal waters in the rest of the ocean, as seen in Fig. 6. Also illustrated in the same figure, the optimal form gives much more reasonable solutions, even with strongly mismatched compressibilities. It remains to be seen whether it is ultimately better to use the original discretization using the pressure at the top of a layer to calculate the compressibility compensated layer density or this optimal form. The original form avoids having resting interfaces that are artificially deformed to reflect the topography, while the optimal form minimizes both the topographically induced excursions of resting interfaces and the propensity for the thermobaric instability to occur. In either case, a horizontally varying reference compressibility dramatically improves the simulations of global isopycnic models using the full nonlinear equation of state.

6. Horizontally varying compressibility corrections.

One way that the thermobaric instability might be avoided would be by defining the compressibility compensation function to be a function of both pressure and horizontal location, i.e. $p^* = F(x, y, p)$ and $\alpha = \alpha^* \partial p^* / \partial p$. Doing so can ensure that compressibility is well compensated everywhere, but it leads to a third pressure gradient term. In this case

$$\alpha^* \nabla_s p^* = \alpha \frac{\partial p}{\partial p^*} \left(\frac{\partial p^*}{\partial p} \nabla_s p + \nabla_p p^* \right) = \alpha \nabla_s p + \alpha^* \nabla_p p^*, \quad (49)$$

so

$$\nabla_p \phi = \nabla_s \phi + \alpha \nabla_s p = \nabla_s \phi + \alpha^* \nabla_s p^* - \alpha^* \nabla_p p^* = \nabla_s (\phi + \alpha^* p^*) - p^* \nabla_s \alpha^* - \alpha^* \nabla_p p^*. \quad (50)$$

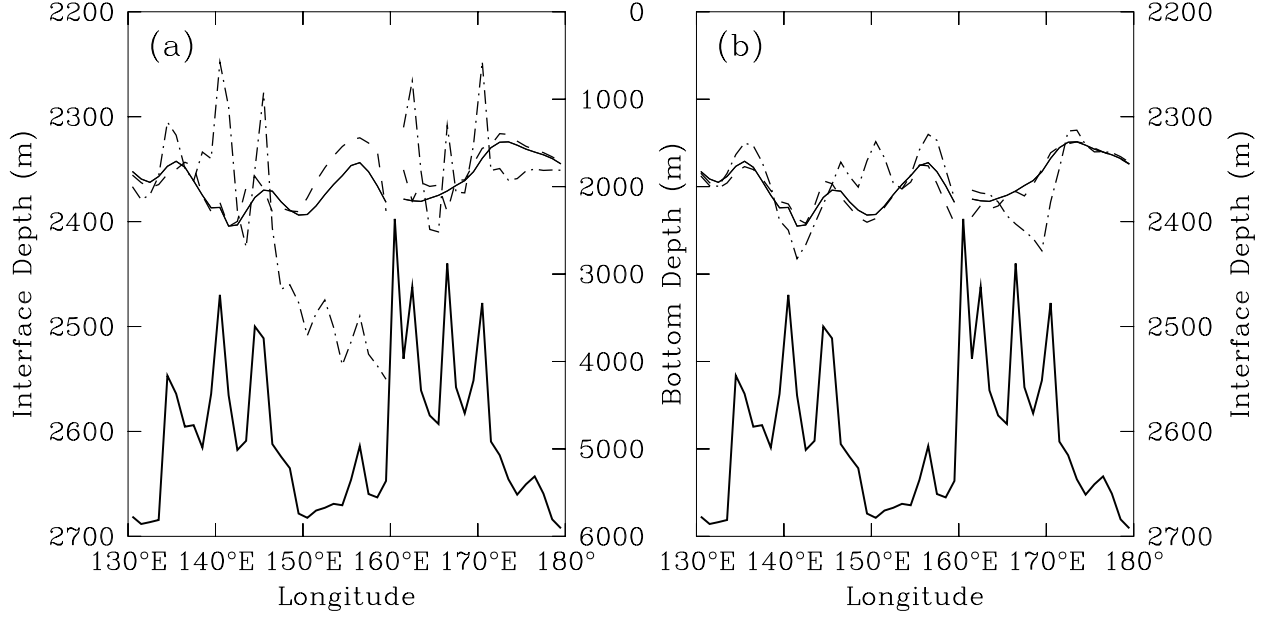


Fig. 6. Height of a selected interface in the abyssal Pacific along 10.5° N using different reference compressibilities and discretizations of the pressure gradient terms. This interface is atop the bottommost layer in much of this section and within a few layers of the bottom in the remainder. The dot-dashed (jagged) lines use a compressibility that is characteristic of the Mediterranean (12° C warmer than the ambient water). The dashed lines use a compressibility that is characteristic of the Weddell Sea (2° C colder than the ambient waters). Panel (a) uses the average layer pressure to calculate the constant layer density (\hat{M}), while (b) uses the optimal Montgomery potential (\hat{M}). The smoother black line in both panels uses a locally appropriate compressibility (by using the spatially varying compressibility described in section 6), and it is indistinguishable regardless of which of the available discretizations are used. The bottom depth along this transect is shown with the very heavy line, using the scale in the middle, which compresses the topography 12-fold relative to the interface height. Note the strong correlation between the spikes in the dot-dashed line in (a) and the topography.

The hydrostatic equation is unchanged by allowing the compressibility compensation to vary with horizontal location,

$$\frac{\partial \phi}{\partial p^*} = \frac{\partial p}{\partial p^*} \frac{\partial \phi}{\partial p} = -\alpha^*, \quad (51)$$

and so is the equation used to calculate the Montgomery potential,

$$\frac{\partial M^*}{\partial \alpha^*} = \frac{\partial}{\partial \alpha^*} (\phi + \alpha^* p^*) = p^*. \quad (52)$$

Although there are three pressure gradient terms in (50) that must be discretized, the third term is not necessarily a great impediment. It is always possible to offset F so that it is a constant at some chosen pressure, \bar{p} . For example, if the compressibility compensation function satisfies (8) for a reference profile for which

$$R = -\frac{1}{\alpha} \frac{\partial \alpha}{\partial p} \Big|_{\theta, S} = \frac{\alpha}{c_s^2}, \quad (53)$$

where c_s is the speed of sound, an appropriate functional form for F is

$$\begin{aligned}
F(p) &= \int_{\bar{p}}^p \exp\left(-\int_{\bar{p}}^{\tilde{p}} R(p) d\tilde{p}\right) d\tilde{p} + \bar{p} \\
&\approx \bar{p} - \frac{1}{R} \left\{ \exp[-R(p - \bar{p})] - 1 \right\}. \\
&\approx p - \frac{1}{2} R(p - \bar{p})^2
\end{aligned} \tag{54}$$

The first approximation here is valid since variations in R are small compared with its mean value, while the second is based on the observation that $R \approx 4 \times 10^{-10} \text{ Pa}^{-1}$, so for typical ocean depths $R|p - \bar{p}| \lesssim (4 \times 10^{-10} \text{ Pa}^{-1})(4 \times 10^7 \text{ Pa}) = 0.016 \ll 1$. Both approximations applied in deriving the second and third lines of (54) are here only for illustration – in practice $F(p)$ might be a direct fit of an analytically integrable function to the exponential inside of the integral on the first line of (54) making any further approximation unnecessary. With these assumptions, the third pressure gradient term becomes

$$\alpha^* \nabla_p p^* \approx -\frac{1}{2} \alpha^* (p - \bar{p})^2 \nabla_p R. \tag{55}$$

The reference compressibility can be forced to vary slowly in space, so that the magnitude of its gradient is small. For typical ocean properties, if the compressibility change due to a 1°C difference in temperature occurs over a horizontal distance of 1000 km, $\nabla_p R \approx 2.5 \times 10^{-18} \text{ Pa}^{-1} \text{ m}^{-1}$, so a typical acceleration from this term evaluated 1000 dbar from the chosen pressure where it vanishes (\bar{p}) is $\alpha^* \nabla_p p^* \approx 1.2 \times 10^{-7} \text{ ms}^{-2}$. Even after discretization, this term will likely be balanced by the other pressure gradient terms (as is mathematically true in the continuous limit), but if (as a worst-case estimate) it is balanced instead by a typical midlatitude Coriolis acceleration, the resultant velocity is only about $1.2 \times 10^{-3} \text{ ms}^{-1}$.

It is possible to further reduce the impact of this third pressure gradient term by minimizing a cost-function based on the volume integrated square of the third pressure gradient term and (motivated by (32)) the inverse stratification weighted misfit between the observed and compensated compressibilities. That is, the cost function should ideally be something like

$$S = \iiint \left(\alpha^* \nabla_p F \right) \cdot \left(\alpha^* \nabla_p F \right) + \Gamma \left[\frac{g^2}{\alpha N^2} \left(\frac{1}{F'} \frac{\partial F'}{\partial p} - \frac{1}{F'_{Obs}} \frac{\partial F'_{Obs}}{\partial p} \right) \right]^2 dV, \tag{56}$$

where Γ is the relative weight of the two terms in units of an acceleration squared. A slightly different stratification weighting should probably be used to avoid singularities in the cost function where the stratification vanishes and to introduce an estimate of the observed variability or uncertainty in the compressibility, but it is useful to emphasize that more heavily stratified regions are much more tolerant of mismatches in the compensation of compressibility. Actually solving for the full three-dimensional compressibility function that minimizes (56) is likely to be overkill.

Instead of minimizing (56), it has been found in practice that an acceptable cost function obtained by first fitting the observed compressibility with a function whose integral with pressure is $F_o(x, y, p)$, and then setting the cost function to be

$$S = \iint D \left(D^2 \nabla F \right) \cdot \left(D^2 \nabla F \right) + \gamma D \left(D^2 (F - F_o) \right)^2 dA, \tag{57}$$

where D is the local depth of the ocean and γ is a relative weight, now with units of an inverse length squared. The D^2 in the first term (57) reflects the dependence of the magnitudes of this additional pressure gradient term on pressure in (55), now assuming that F is chosen to be

constant at $p=0$, while in the second term the D^2 is simply a guess based on the observation that the ocean's stratification is far weaker deeper in the abyss than near the surface. The F'' anomalies in (56) are replaced with anomalies in F in (57) so that the equation will become separable; this is justified by noting from (54) that the leading order anomalies in F are quadratic in pressure. The model performance is not found to vary much with changes to either the value of γ or even to the power of D in the second term in (57). Choosing (57) as the cost function effectively concentrates the significant gradients into shallow areas (such as Gibraltar) where the third pressure gradient term has a minimal impact on the solution, while ensuring that the broad spatial variations of compressibility are reasonably well captured.

The minimum of the cost function (57) is the steady-state solution of the equation

$$\frac{\partial F}{\partial t} = \frac{L^2}{TD^5} \nabla(D^5 \nabla F) + \frac{\gamma L^2}{T} (F - F_o). \quad (58)$$

If F follows the same functional form as F_o and that functional form is chosen to be the sum of horizontally varying fit coefficients times nonlinear but analytically differentiable vertical functions of pressure, (58) has the virtue that the optimal fit coefficients are independent of pressure. The minimization need not be perfect, so (58) only needs to be integrated long enough to suppress the smaller scales. Eq. (58) can be iterated independently for each of the fit coefficients for the same amount of time, and the resulting smooth function will be the solution to (58) at every pressure.

In practice, the compensation for the third pressure gradient term in (50) does appear to occur almost entirely within the other pressure gradient terms. In the 48-layer global example, there is very little difference between simulations with reference compressibilities generated using $\gamma = (10^6 \text{ m})^{-2}$ and $\gamma = (10^4 \text{ m})^{-2}$, even though there is typically a 4-fold difference in the magnitude of the third pressure gradient term. (The velocity differences are of typically order of 10^{-4} m s^{-1} out to a few tens of days, at which point nonlinearities make exact comparison less meaningful.) This result provides strong assurance that the full nonlinear equation of state can be used without an excessively strong dependence on the details of the reference compressibility that is being extracted.

7. Discussion: Avoiding the thermobaric instability.

There are a number of ways that the thermobaric instability can be avoided. Some of these have been mentioned previously in this manuscript, but they will be mentioned again here to present all of the options in the same context.

Thermobaricity can be avoided altogether. This is essentially what is done when a potential density is used for both the coordinate variable and for calculating pressure gradient accelerations (e.g. Oberhuber, 1993). As discussed earlier, this introduces significant errors in the model's thermal wind shear (Sun et al., 1999). Eden and Willebrand (1999) suggest that by using a regional fit to observed properties to obtain a quasi-neutral density variable that is a function only of potential temperature and salinity, thermal wind shears and buoyancy frequency can be evaluated quite accurately without consideration of thermobaricity. While this works well in a North Atlantic simulation (Eden and Willebrand, 1999) (and probably would work equally

well in other regional simulations) it is problematic for global simulations and for long simulations in which the regional watermass structure can change.

In isopycnic coordinate models, it is always an option to choose the layer target densities to avoid resolving the internal structure of very weakly stratified watermasses with anomalous properties. In fact, since the target layer densities are chosen a priori, it is always possible to limit the minimum resolvable stratification. For example, suppose that the smallest permissible stratification that is desired in the coarse-resolution version of (32) is $N_{\min, \text{Eff}}^2 \approx 4 \times 10^{-7} \text{ s}^{-2}$, which would give a roughly 6K range of stability (adequate for the open ocean). Stability can then be ensured if the smallest prescribed density difference between layers is

$$\Delta\rho_{\text{Min}} = N_{\text{Min, Eff}}^2 P_{\text{Max}} / g^2 \approx (4 \times 10^{-7} \text{ s}^{-2})(4 \times 10^7 \text{ Pa}) / (9.8 \text{ m s}^{-2})^2 \approx 0.17 \text{ kg m}^{-3}. \quad (59)$$

This is not much coarser than resolutions typically used in models with relatively few layers, but of course such density differences preclude resolution of the structure in weakly stratified regions. It is possible to use finer resolution, provided that any weakly stratified regions that are then resolved have compressibilities that are close to the reference value. For example, Sun and Bleck (2001) have successfully run a global model using the full nonlinear equation of state and the Sun et al. (1999) treatment of thermobaricity without encountering the thermobaric instability. But with only 15 interior layers, none of which capture the structure of the deep Mediterranean, they avoid altogether the possibility that the interior Mediterranean would be unstable. They do choose layers that describe the density of the Weddell sea, but the Sun et al. (1999) techniques essentially extract a compressibility characteristic of a water column with a uniform temperature and salinity of 0°C and 35 psu. These values are close enough to the properties found in the Weddell Sea to avoid instability. Subsequent HYCOM simulations using the Sun et al. (1999) treatment of compressibility with higher vertical resolutions in the density range of Labrador Sea water [which at its source is very weakly stratified and has temperatures that have ranged over the twentieth century between 2.7 and 3.6°C, (Dickson et al., 1996)] do appear to exhibit this instability (A. Wallcraft, pers. comm.). The illustrations of the instability presented in the current paper used 45 interior isopycnal layers, including some with densities specifically chosen to resolve the vertical structure of both the Mediterranean and Weddell Seas.

Orthobaric density (de Szoek et al., 2000) is derived by fitting the observed sound speed (essentially the compressibility) as a function of *in situ* density and pressure. Because of salinity variations in the ocean, this can never be perfect, but with the added degrees of freedom from a fit in two-dimensions, the typical standard deviations of sound speeds from the fit are less than 5 m s^{-1} (roughly equivalent to 1°C) below the top few hundred meters (de Szoek et al., 2000). The thermobaric instability could only occur in weakly stratified water masses with atypically large salinity anomalies, but as weakly stratified watermasses tend to be heavily weighted in the fitting procedure, this is unlikely. Using orthobaric density for both the coordinate variable and for calculating pressure gradients will likely avoid the instability described here. Although there are other considerations apart from the calculation of pressure-driven accelerations (such as non-materiality of the coordinate variable and a larger departure from current practice) that also arise from using orthobaric density, it is a promising approach that should be further explored for use in Lagrangian vertical coordinate modeling.

It might be possible to suppress the thermobaric numerical instability by choosing a maximal estimate for compressibility, so that the instability would always appear as a negative apparent reduced gravity between layers. It is easy to catch instances of negative apparent reduced

gravities, and the consequences can then be avoided by artificially adjusting the α^* of one of the layers. This would have the effect of altering the apparent stratification of the water column and locally increasing the internal gravity wave speeds. This would seem to be an undesirable option, as it alters the physics of the solution, even in instances where compensation between the two pressure gradient terms would stabilize the solution anyway.

Finally, it has been demonstrated here that the combination of a more careful treatment of the discretization of the pressure gradient terms and extracting a slowly horizontally varying reference compressibility eliminates the thermobaric instability in a global isopycnic model simulation of the current ocean state, even one with high resolution in density space. Each of these two measures alone may be adequate in some circumstances. Using the optimal discretization of the pressure gradient term is likely to be sufficient in regional simulations where the horizontal variations of compressibility are not especially large. In global models with coarse resolution in density or small temporal variations of the compressibility, the current discretizations can probably be used effectively when a spatially varying compressibility is extracted. The two measures taken together provide a robust solution to the thermobaric instability, useful even for global ocean simulations with high resolution in density.

The price of the more careful discretization of the pressure gradient term is that the resting isopycnal depths will weakly reflect the bottom topography, and there will be a weak abyssal flow unless compressibility is well compensated. But note that if compressibility is perfectly compensated, the changes to the discretization have no effect at all.

The price of extracting a spatially varying reference compressibility from the pressure gradient calculations is that a third pressure gradient term enters the equations of motions. Like the second term, this term is solenoidal, but it can be made small by choosing the reference compressibility to vary slowly in the horizontal. By adding this third term, both the second and third terms can be made much smaller than the along-coordinate gradient of the Montgomery potential, and the cumulative truncation errors will be much smaller than the physical pressure gradient acceleration. In adding this spatially varying compressibility, it could be argued that the “correct” state of the ocean is somehow being fed to the model, but in the continuous limit none of the modifications suggested here change the equations being solved. In addition, if this approach is used in a very long simulation in which the state of the ocean drifts substantially, it is always possible to periodically re-fit the reference compressibility, provided that there is a gradual change between old and new reference compressibilities to avoid an excessively vigorous adjustment.

With the new developments presented here, built upon the insights of Sun et al. (1999), or the orthobaric density techniques of deSzoeke et al. (2000), it is very likely that difficulties with the calculation of pressure gradient accelerations with the full nonlinear equation of state will no longer present a compelling barrier to the use of Lagrangian vertical coordinate ocean models in realistic applications.

Acknowledgements. Brian Arbic assisted with some Mediterranean-only simulations that demonstrated that the thermobaric instability previously identified in the Weddell Sea of a Southern Hemisphere simulation was also the root of the difficulties we were having with our global model. I would also like to thank Stephen Griffies for his assistance with the calculus of variations derivation of (58). Both also provided thorough internal reviews. I would also like to

thank Rainer Bleck, Eric Chassignet, Roland deSzoeke, Anand Gnanadesikan, Scott Springer, Shan Sun, and Alan Wallcraft for useful conversations on this matter, along with two referees for their quick and useful suggestions on the manuscript.

REFERENCES:

- Bleck, R., 1998: Ocean modeling in isopycnic coordinates. In *Ocean modeling and parameterization*, E. P. Chassignet and J. Verron eds., Kluwer, 423-448.
- Bleck, R., 2002: An oceanic general circulation model framed in hybrid isopycnic-Cartesian coordinates. *Ocean Modelling*, **37**, 55-88.
- de Szoeke, R. A., 2000: Equations of motion using thermodynamic coordinates. *J. Phys. Oceanogr.*, **30**, 2814-2829.
- de Szoeke, R. A., S. R. Springer, and D. M. Oxilia, 2000: Orthobaric density: A thermodynamic variable for ocean circulation studies. *J. Phys. Oceanogr.*, **30**, 2830-2852.
- Dickson, R., J. Lazier, J. Meincke, and P. Rhines, 1996: Long-term coordinated changes in the convective activity of the North Atlantic. In *Decadal climate variability: dynamics and predictability*, D. L. T. Anderson and J. Willebrand eds., Springer-Verlag, 211-262.
- Eden, C., and J. Willebrand, 1999: Neutral density revisited. *Deep-Sea Res. II*, **46**, 33-54.
- Gill, A. E., 1982: *Atmosphere-Ocean Dynamics*, Academic Press, 662 pp.
- Hallberg, R., and A. Gnanadesikan, 2001: An exploration of the role of transient eddies in determining the transport of a zonally reentrant current. *J. Phys. Oceanogr.*, **31**, 3312-3330.
- Hallberg, R., and P. Rhines, 1996: Buoyancy-driven circulation in an ocean basin with isopycnals intersecting the sloping boundary. *J. Phys. Oceanogr.*, **26**, 913-940.
- Levitus, S., T. P. Boyer, M. E. Conkright, T. O'Brien, J. Antonov, C. Stephens, L. Stathoplos, D. Johnson, and R. Gelfeld, 1998: *World Ocean Database 1998. Volume 1: Introduction*. NOAA Atlas NESDIS 18, 346 pp.
- Lin, S.-J., 1997: A finite-volume integration method for computing pressure gradient force in general vertical coordinates. *Q. J. R. Meteorol. Soc.*, **123**, 79-1762.
- Mellor, G. L., and X. H. Wang, 1996: Pressure compensation and the bottom boundary layer. *J. Phys. Oceanogr.*, **26**, 2214-2222.
- Oberhuber, J. M., 1993: Simulation of the Atlantic circulation with a coupled sea ice - mixed layer - isopycnal general circulation model. Part I: Model description. *J. Phys. Oceanogr.*, **23**, 808-829.
- Sun, S., R. Bleck, C. G. H. Rooth, J. Dukowicz, E. P. Chassignet, and P. Killworth, 1999: Inclusion of thermobaricity in isopycnic-coordinate ocean models. *J. Phys. Oceanogr.*, **29**, 2719-2729.
- Sun, S., and R. Bleck, 2001: Thermohaline circulation studies with an isopycnic coordinate ocean model. *J. Phys. Oceanogr.*, **31**, 2761-2782.
- Williams, R. G., and V. Roussenov., 2003: The role of sloping sidewalls in forming potential vorticity contrasts in the ocean interior. *J. Phys. Oceanogr.*, **33**, 633-648.